J. Hydrol. Hydromech., 70, 2022, 2, 244–256
https://doi.org/10.2478/johh-2022-0013

sciendo Journal of Hydrology and Hydromechanics Institute of Hydrology SAS

Field-scale assessment of the unsaturated hydraulic properties of residual soils in southeastern Brazil

Ruan G.S. Gomes[1*], Guilherme J.C. Gomes[2,3], Eurípedes A. Vargas Jr.[1], Martinus Th. van Genuchten[4,5], João T.M.G. Pinto[1], Felipe A. Rosa[1]

[1] Department of Environmental and Civil Engineering, Pontifical Catholic University of Rio de Janeiro, Brazil.
[2] Department of Environmental Engineering, Federal University of Ouro Preto, MG, Brazil.
[3] Graduate Program in Geotechnics, School of Mines, Federal University of Ouro Preto, MG, Brazil.
[4] Department of Earth Sciences, Utrecht University, Netherlands.
[5] Department of Nuclear Engineering, Federal University of Rio de Janeiro, RJ, Brazil.
[*] Corresponding author. E-mail: ruan_gomes93@hotmail.com

Abstract: Field tests were carried out to estimate effective unsaturated soil hydraulic properties of layered residual soils in Rio de Janeiro, southeastern Brazil. Data of this type are important for understanding the initiation of rainstorm-induced soil landslides, which often occur in the state of Rio de Janeiro as well as other areas having similar geologic settings and climate conditions. Tests were carried out using a simplified field approach, referred to as the Monitored Infiltration Test, which requires only a tensiometer to measure pressure heads below the wetting front, triggered by flow from a Mariotte bottle which maintains a constant pressure at the top edge of the soil profile. The data can then be analyzed by numerical inversion using the HYDRUS-2D software package. The test is relatively fast since no steady-state flow conditions are needed, and versatile since the test can be carried out quickly on steep slopes with the help of a manual auger. Soil water retention and the unsaturated hydraulic conductivity functions were obtained for a range of young, mature and saprolitic residual soils. The effective hydraulic properties of the distinct residual soil layers can be quite large, reflecting a need to provide a careful analysis of field-scale hydraulic heterogeneity in geotechnical analyses.

Keywords: Residual soils; Unsaturated soil hydraulic properties; Field infiltration tests; HYDRUS-2D.

INTRODUCTION

Residual soils are found in many humid tropical regions where weathering of the parent rock is more intense and extended to greater depths than in other parts of the world (Bells, 2005). Characterization of the unsaturated hydraulic properties of such soils is challenging because of soil heterogeneities that are strongly controlled by relict discontinuities. In Brazil, the weathering profile of residual soils encompasses layers derived from granites, gneisses, and basalts (Lacerda, 2010). These layers have been classified mostly as (i) mature, (ii) young and (iii) saprolitic residual soils (Gerscovich et al., 2006). Fig. 1 shows a typical weathering profile of many gneissic regions of Brazil, such as in the state of Rio de Janeiro. Mature soils are traditionally found in the uppermost part of a residual soil, relatively close to organic layers where plant roots are often present. These soils are often fine-textured because of weathering (i.e., through the process of laterization). Residual young soils, usually found in deeper layers, are in an earlier stage of weathering as often reflected by small relic structures in their skeleton. Residual saprolitic soils represent that part of the weathered profile where the soil strongly preserves the microfabric and volume of the underlying fresh bedrock (Aydin, 2006).

Heterogeneities of the different soil layers may significantly modify pressure head distributions in residual soil slopes during rainfall infiltration (Kassim et al., 2012). Although numerous studies performed stability analyses of catchments involving residual soils (Camargo et al., 2016; Gomes et al., 2017), relatively few have examined the heterogeneous nature of subsurface flow processes at the watershed spatial scale (Li et al., 2016). The lack of soil hydraulic property data to be used as

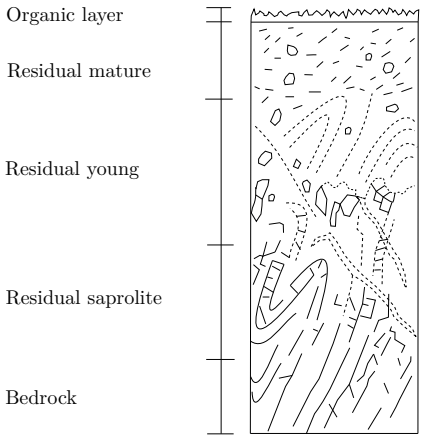

Fig. 1. Representative weathering profile of the residual soils in Rio de Janeiro, Brazil.

effective properties of heterogeneous soil domains is a major problem limiting field-scale analyses (Liang and Uchida, 2014), especially of areas that are susceptible to landslides.

Several studies previously estimated the hydraulic properties of residual soils. For example, Kassim et al. (2012) investigated pressure head distributions of a two-layered residual soil slope in Malaysia. By comparing numerical simulations with field measurements, they found that residual soils with relict discontinuities, such as saprolitic soils, should be subdivided into multiple zones with effective (average) soil hydraulic properties. Recently, Peranić et al. (2018) estimated the water retention functions of residual soils from flysch rock mass

using six different field and laboratory methods. Despite their sampling covering depths of only about 0.5 to 1 m of a relatively small watershed, they indicated that the derived data considerably improved their studies of rainfall-induced landslides in flysch slopes. More precise definition of soil hydraulic properties of landslide-prone regions should improve simulations of shallow landslides and debris-flows (Gomes et al., 2016; Rahardjo and Satyanaga, 2019). Unfortunately, the effective hydraulic properties of layered residual soils are largely unknown in regions susceptible to landslides such as occur often in Rio de Janeiro state (Fernandes et al., 2004; Gomes et al., 2017; Vieira and Fernandes, 2004).

The main purpose of this paper is to obtain field-experimental data to derive effective water retention and unsaturated hydraulic conductivity functions of mature, young and saprolitic residual soils of landslide-prone regions in Rio de Janeiro, Brazil. The field data were obtained using an approach, coined here as the Monitored Infiltration Test, similar to that of a tension disc infiltrometer but much simpler by requiring only a tensiometer and a Mariotte bottle. Moreover, the test is fast since inverse modeling of the pressure head data does not require steady state flow, while the device can be installed quickly on steep slopes with the help of a manual auger. The approach was conceptualized initially by Velloso (2000), who through numerical analysis demonstrated its feasibility and adequacy for determining van Genuchten (1980) model parameters. Our field tests use a tensimeter to measure pressure heads below a Mariotte bottle, which maintains a constant pressure head at the upper boundary condition during the experiment. Measured data are subsequently analyzed by numerical inversion using the HYDRUS-2D software package (Šimůnek et al., 2016).

The estimated soil hydraulic properties will be contrasted against results obtained from different field and laboratory experiments. We emphasize here that the attention in our study is on direct field measurements. Laboratory tests such as various outflow and evaporation methods (e.g., Chen et al., 2017; Peters et al., 2015) have the advantage of being relatively fast and precise (Scharnagl et al., 2011). Unfortunately, laboratory tests on small soil samples may be inappropriate to characterize soil water dynamics at the field spatial scales (Peranić et al., 2018; Vrugt et al., 2008). Inverse modelling of field data facilitates more accurate, rapid, reliable, and cost-effective estimation of the hydraulic properties of the considered soil domain (Šimůnek et al., 2012; Vrugt et al., 2004). They do not necessarily require steady-state flow conditions, can be adapted to many laboratory conditions or large-scale field flow scenarios, and provide estimates of parameters uncertainty. For our study we used the observed pressure head data to estimate the hydraulic properties of steeply sloping residual soils that are frequently subjected to landslides (Gerscovich et al., 2006; Peranić et al., 2020).

MATERIALS AND METHODS

Fig. 2 provides a flowchart of the methodology used to estimate the hydraulic properties given by the water retention, $\theta(h)$, and the hydraulic conductivity, $K(h)$ functions, where θ is the volumetric water content, K the hydraulic conductivity, and h the pressure head. The framework involves four main steps: transient measurements of pressure heads using the monitored infiltration test, inverse modeling, evaluation of the fitted $\theta(h)$ and $K(h)$ functions relative to other methods, and classification of the effective soil hydraulic properties of residual soils. Details are given in the next subsections.

Field site

Field investigations were carried out at five locations in Rio de Janeiro, Brazil (Fig. 3). Geographic locations of the sites are depicted with colored boxes, representing mature (green), young (red) and saprolitic (blue) residual soils. The locations Campo Grande (L1), Joá (L2), Duque de Caxias (L3), Rio Bonito (L4), and Nova Friburgo (L5) were selected to maximize information about the residual soils in Rio de Janeiro. Those have been studied extensively by many before, especially after unusually large mass movements in 1996 (e.g., Fernandes et al., 2004; Gerscovich et al., 2006; Gomes et al., 2008, 2016, 2017; Vieira and Fernandes, 2004) and 2011 (Rosi et al., 2019).

The local geology consists of high-grade metamorphic rocks (mostly Archer gneiss) with granite intrusions of coarse to medium granular texture (Fernandes et al, 2004; Gomes et al., 2016; Vieira and Fernandes, 2004). Human impacts in the area are limited to a few small residential areas, while vegetation (of the Atlantic Forest) has been preserved in many places (Gomes et al., 2016), particularly around the Joá (L2) and Nova Friburgo (L5) sites. Irregular urbanization in other areas such as Campo Grande (L1), Duque de Caxias (L3) and Rio Bonito (L4) have had a considerable negative impact on the generation of rainfall-induced landslides (Fernandes et al., 2004; Rosi et al., 2019). The mountainous region of Rio de Janeiro in general has been vulnerable to landslides. For example, thin weathered regolith zones on steep slopes are frequently subject to mass movements. The highly fractured lithology enables preferential infiltration paths and, consequently, rapid development of positive pore water pressures within the soil mass (Gerscovich et al., 2006). In addition, intense summer rainstorms in Rio de Janeiro exert a strong control on slope stability via infiltrating water, which increases pore pressures within the soil and decreases the shear strength (Fernandes et al., 2004; Gomes et al., 2017). We refer to the cited publications for more detailed descriptions of the field sites.

Monitored infiltration test

The field monitored infiltration test relies on a simple geometry of the experimental setup, which maintains a constant hydraulic head that triggers infiltration into the soils leading to temporal changes in the pressure head recorded with a tensiometer installed below an excavated soil pit. The setup allows pressure head measurements within the created water bulb, which extends to a few centimeters. Tensiometric pressure head data are used since they generally provide sufficient information to guarantee correct assessment of the soil hydraulic properties (Šimůnek and van Genuchten, 1996; Velloso, 2000). Fig. 2 (upper block) provides a general overview of the proposed methodology. A full description of the test setup is shown in Fig. 4.

The first step is cleaning and levelling the tested location to enable the excavation of a cylindrical pit with the help of a bucket auger (Fig. 4a). For the excavation we used a bucket auger with a diameter of 10.16 cm. After excavation and cleaning, the exact dimensions of the pit are recorded for use in subsequent numerical simulations. To later accommodate a Mariotte bottle in the excavated pit, we recommend a radius (r_R) of 10 to 20 cm, and a depth (z_D) of approximately 20 to 30 cm to impose a constant hydraulic head.

The second step consists of opening an adequate small cavity to install the tensiometer (although other devices may be used to measure pressure heads and/or the water contents).

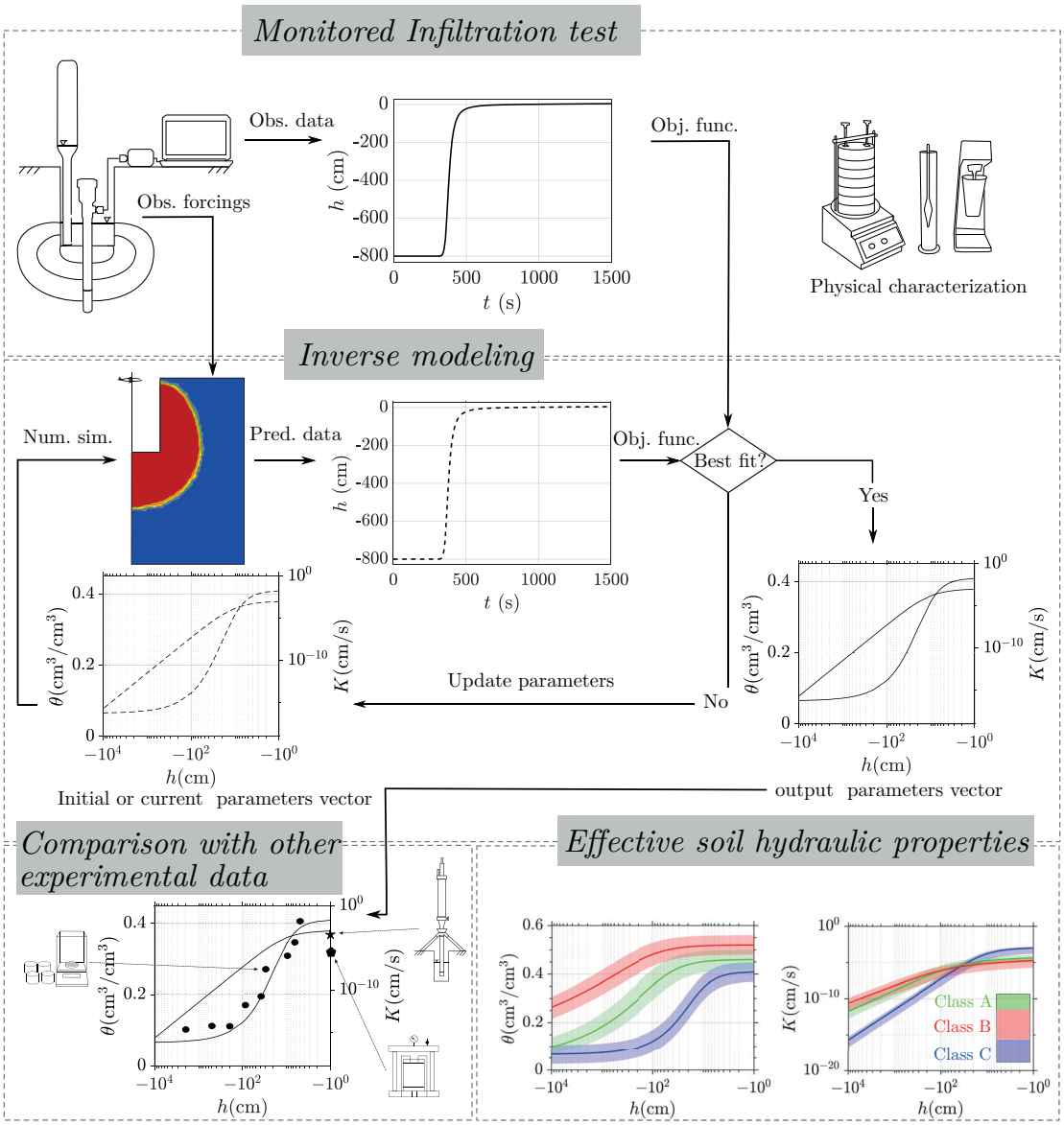

Fig. 2. Schematic of the different steps of the proposed framework for estimating the effective soil hydraulic properties. The top panel details the different experimental steps of our monitored infiltration test following the initial conceptualization of Velloso (2000). The middle panel summarizes inverse modeling of the pressure head, h, data using the HYDRUS-2D software to estimate the soil hydraulic parameters. The bottom panel illustrates comparisons of the estimated $\theta(h)$ and $K(h)$ functions with independent experimental data (left) and a graphical illustration of the effective soil hydraulic properties of the residual soils (right).

The tensiometer holes in our study were created with a helical auger as indicated in Fig. 4b. The tensiometers can be installed at different depths and at different radial distances from the center axis of the cylindrical soil pit. Fig. 4c, shows three different configurations: vertical (v), radial (r) and horizontal (h). Having these options makes the test more flexible to field conditions, such as for instance to capture degrees of anisotropy by combining vertical and radial flow measurements. We found the radial configuration of the tensiometer to be the simplest to execute. Vertical positioning is more delicate to implement, while the horizontal configuration is more time consuming since it requires the drilling of an additional hole. Still, the horizontal configuration may be more suitable for sloping terrains. Although we used for our study only one tensiometer, we note that the inverse optimization with HYDRUS-2D allows the use of multiple monitoring devices (for water contents and/or pressure heads) at multiple locations. After installing the tensiometer and the data logger, the water-filled tensiometer will lose initially some moisture to the unsaturated soil until the (negative) pressure head inside the tensiometer cup at some location (r_T, z_T) equals the pressure head of the surrounding soil.

The next stage is installation of the Mariotte bottle. As indicated in Fig. 4d, the Mariotte bottle must be placed carefully inside the open pit to enable establishing a water column inside the pit to trigger the infiltration process. The last phase is then to open the Mariotte bottle valve to impose a hydraulic head (Fig. 4e). Typically, a few seconds are required for the water level to reach the desired height (z_H), which is then the imposed boundary condition for the HYDRUS simulations. As infiltration commences, initial soil water pressure heads will increase. The infiltration front eventually reaches the tensiometer ceramic capsule, at which time the pressure head at that location will increase and eventually plateau to a constant value, at which time the test may be terminated. Disturbed and/or undisturbed

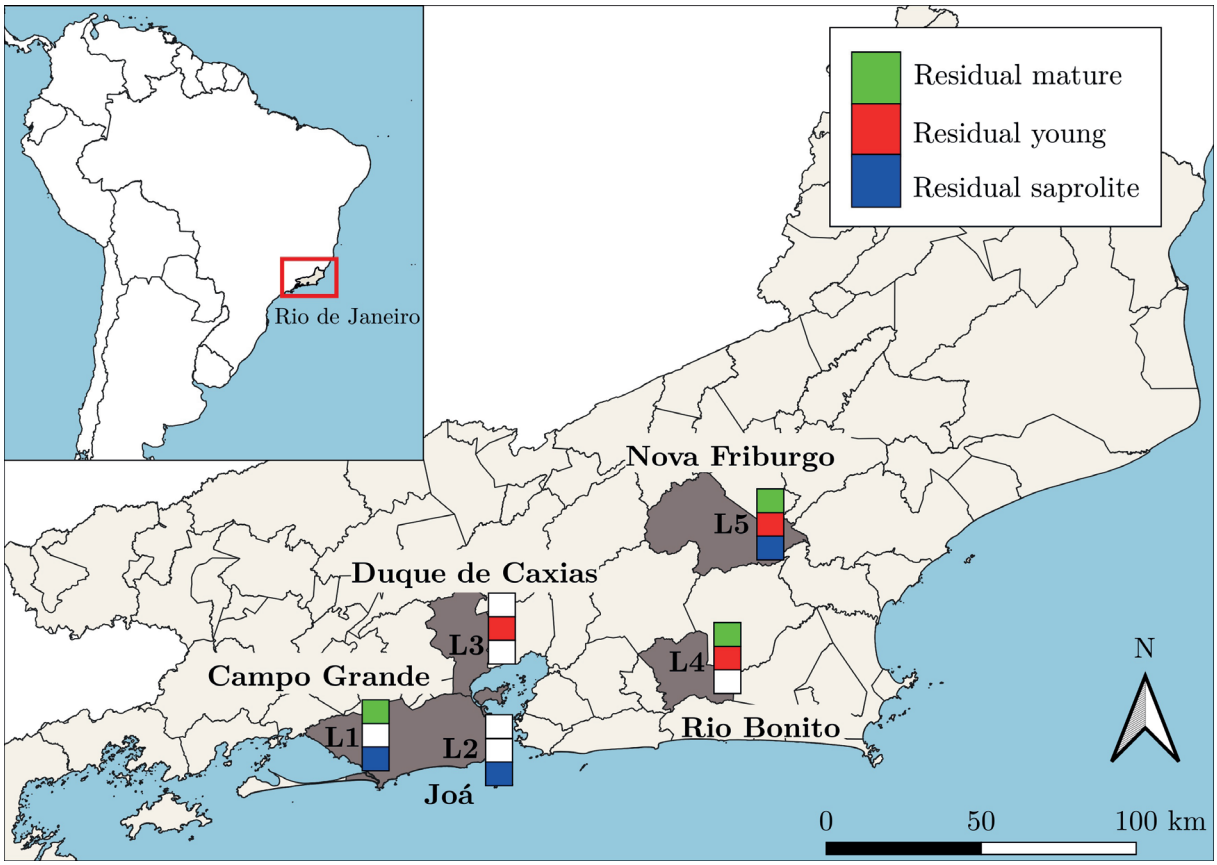

Fig. 3. Geographic overview of the experimental field sites in the Brazilian state of Rio de Janeiro. The coloured boxes denote specific sites where investigations were carried out on mature (red), young (green) and saprolitic (blue) residual soils.

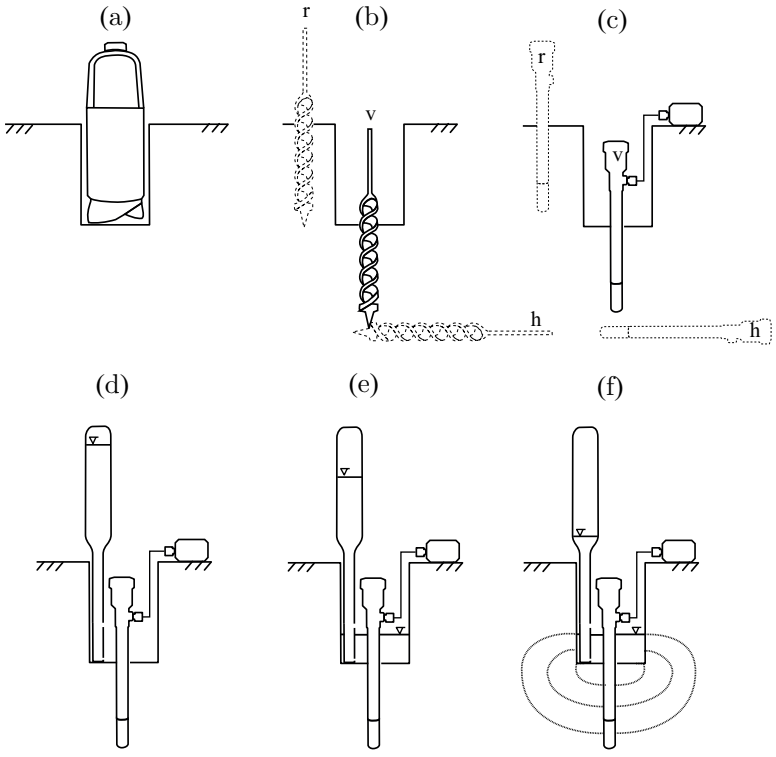

Fig. 4. Consecutive steps of the monitored infiltration test. (a) Opening of the main cylindrical hole using a bucket auger; (b) opening of the tensiometer hole with a helical auger, using three possible configurations: vertical (v), horizontal (h) and radial (r); (c) installation of the tensiometer at the desired position; (d) installation of a Mariotte bottle inside the excavated pit; (e) opening of the valve of the Mariotte bottle to establish a constant hydraulic head and to trigger the infiltration process; (f) measurement of the pressure head (h) until the infiltration front passes the ceramic capsule of the tensiometer and no more changes in h is observed.

samples could still be collected for investigations afterwards, such as in our case by using several samples for further physical characterizations according to Brazilian standards (ABNT, 2016a, b). Fig. 5 summarizes the geometric setup of the monitored infiltration test and the data that must be recorded for subsequent use in the numerical simulations: the depth (z_D) and radius (r_R) of the cylindrical pit, the tensiometer coordinates (r_T, z_T) and the hydraulic head (z_H).

Inverse modeling

As illustrated by the dashed plot in the middle panel of Fig. 2, the monitored infiltration test will lead to an approximatly S-shaped curve of the pressure head h as a function of the time, t. This curve can be numerically simulated using the axisymmetric formulation of the Richards equation in terms of the radial (r) and vertical (z) coordinates:

$$\frac{1}{r}\frac{\partial}{\partial r}\left[rK(h)\frac{\partial h}{\partial r}\right]+\frac{\partial}{\partial z}\left(K(h)\frac{\partial h}{\partial z}-K(h)\right)=\frac{\partial\theta(h)}{\partial t} \tag{1}$$

In this paper, we limited the analyses to isotropic conditions as implied by Eq. (1). The Hydrus-2D finite element code of Šimůnek et al. (2016) was used to numerically solve Eq. (1) for the geometry shown in Fig. 6. The spatial domain (Ω) for this purpose was divided into 1 cm triangular elements, which provided convergence of the results for all cases we considered. The initial condition was assumed to be a constant pressure head equal to the initial reading of the tensiometer. As boundary conditions was imposed a prescribed (Dirichlet) total head z_H along the walls of the wetted part of the excavated soil pit, and no-flow (Neumann) type condition along the remaining boundary nodes. The observation point (red circle in Fig. 6) was set according to the tensiometer ceramic capsule coordinates (r_T, z_T). The lower and the right-hand side boundaries were located sufficiently distant from the infiltration source and the observation point so they did not affect the simulated infiltration process. Overall, a lower boundary of 50 cm, and 40 cm on the right-hand side, may be sufficient to avoid boundary issues. In our experimental and inverse modeling approach, each of the three residual soils (mature, young and saprolitic) was considered to be homogeneous across the entire field site, albeit possibly covering different depths at the various locations.

Table 1 reports the geometry of the pits at each of the five locations (L1 through L5) used as case studies in this paper. Multiple tests were executed at each location. The tests were coded to simplify presentation of our data. For instance, code L1.2 in the second column refers to sample 2 at location L1, etc. Columns five to seven in Table 1 indicate positions of the tensiometer and their coordinates. The last two columns list the initial pressure heads captured by the tensiometer after establishing hydraulic equilibrium, and the total pressure head (z_H) used as Dirichlet condition along the pit boundaries. Note that the initial condition (h_0) varied from –780 to –250 cm, while the imposed top boundary conditions inside the borehole exhibited total water pressures from 3.5 cm to 20.0 cm.

Numerical solutions of Eq. (1) also require knowledge of the hydraulic properties of the residual soil. We used for this purpose the van Genuchten-Mualem (VGM) soil water retention, $\theta(h)$, and hydraulic conductivity, $K(h)$, functions (van Genuchten, 1980) given by

$$S_e(h)=\frac{\theta(h)-\theta_r}{\theta_s-\theta_r}=\begin{cases}\left[1+|\alpha h|^n\right]^{-m}, & h<0\\ 1, & h\geq 0\end{cases} \tag{2}$$

$$K(h)=K_sS_e(h)^L\left[1-\left(1-S_e(h)^{\frac{1}{m}}\right)^m\right]^2 \tag{3}$$

where S_e (–) is effective saturation, θ_r and θ_s (cm^3 cm^{-3}) represents the residual and saturated water contents, respectively, α (cm^{-1}) is a proxy of the reciprocal of the air-entry pressure, n and $m=1-1/n$ are quasi-empirical shape parameters, and K_s (cm s^{-1}) is the saturated hydraulic conductivity. We make the common assumption that L = 0.5 (van Genuchten, 1980), which allows us to use the VGM parameter vector $\boldsymbol{\beta}=\{\theta_r,\theta_s,\alpha,n,K_s\}$ to characterize the hydraulic properties of the residual soils of Rio de Janeiro. The soil hydraulic parameters were estimated using inverse modeling from observed transient pressure head data. Inverse modeling can be understood as the process of iteratively adjusting model parameters to merge as much as possible the observed, $\tilde{\boldsymbol{H}}=\{\tilde{h}_1,\ldots,\tilde{h}_N\}$, and simulated, $\boldsymbol{H}=\{h_1,\ldots,h_N\}$, datasets of dimension N

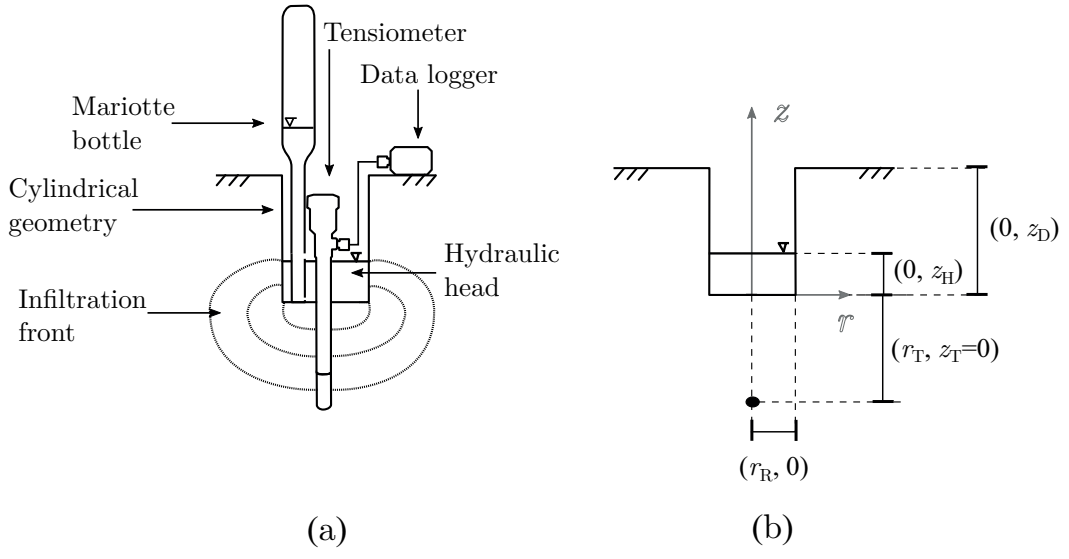

Fig. 5. Schematic overview of the experimental setup of the monitored infiltration test (a) and required geometry data (b).

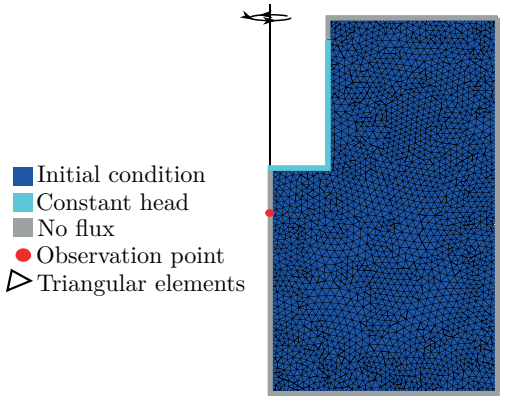

Fig. 6. Representation of the 2D axisymmetric finite element mesh composed of triangular elements. The boundary conditions of Equation (1) are defined at the edges of the mesh of our flow domain. Constant pressure head is used as boundary condition at the excavated part of the soil pit, assuming equilibrium from the lowest located nodal point. A no-flow boundary condition, is assumed at the top, bottom and at the lateral faces of the soil domain. The observation point is separately indicated with a red circle.

(Vrugt et al., 2008). This general idea is denoted as follows:

$$\tilde{\boldsymbol{H}} \approx \boldsymbol{H}\left(\Phi, \tilde{\boldsymbol{X}}, \boldsymbol{\beta}\right) \tag{4}$$

where Φ is the mathematical model that describes the physical process (i.e., the Richards equation in our case), $\tilde{\boldsymbol{X}}$ represents the observed forcing conditions (i.e., boundary conditions), and $\boldsymbol{\beta}$ is the vector of model parameters that are target values within the inverse modeling framework. The soil hydraulic parameters were determined using the iterative Levenberg-Marquardt algorithm as implemented in the HYDRUS software package (Šimůnek et al., 2012, 2016) and illustrated graphically in Fig. 2 (middle panel).

Inverse modeling is based upon minimization of an appropriate objective function, reflecting deviations between the observed values and the predicted system response. In the absence of measured data, we used the Rosetta pedotransfer functions of Schaap et al. (2001) to estimate initial values of the VGM parameters from measured sand, silt, and clay percentages, and the bulk density. Previous studies have shown that the residual water content θ_r is generally the least sensitive of the VGM parameters to the calibration data (e.g., Inoue et al., 1998; Šimůnek et al., 1998; Vrugt et al., 2001). We note here that our tensiometers could not collect pressure head data below about –8 m. Following Vrugt et al. (2001) and others, we fixed the saturated water content, θ_s, at the porosity value, while recognizing that field-saturated water contents often are 10 to 15% lower than porosity because of air entrapment (e.g., Gonçalves et al., 2019). The water bulb generated during the field tests had similar shapes for flat and sloping terrains.

Comparison with other experimental data

Monitored infiltration test results were compared with a series of well-established soil physical and other tests to characterize the sampled soils. Tests included the filter paper technique following ASTM (2013), measurements of the saturated hydraulic conductivity using a laboratory flexible wall permeameter in accordance with ASTM (2016), and field Guelph permeameter measurements (Reynolds and Elrick, 1986). The tests supplied independent data to provide insights about the accuracy of the inverse modeling approach.

Effective soil hydraulic properties

Our main objective was to obtain effective VGM soil hydraulic parameters of residual soils in Rio de Janeiro. Effective soil hydraulic properties are defined here as the $\theta(h)$ and $K(h)$ functions that create averaged responses of the actual heterogeneous residual soil class. For this purpose we grouped the optimized soil hydraulic parameters of each soil class as shown in Fig. 3. This allowed us to estimate the mean and 95% confidence intervals of the water retention and hydraulic conductivity functions of the mature, young and saprolitic residual soils of Rio de Janeiro, as illustrated in Fig. 2 (bottom panel).

Table 1. Summary of the experimental conditions used in the field tests, including sample code, geometry of the boreholes, radial coordinates of the tensiometers, and the initial, and inflow boundary conditions. All numerical values are expressed in cm.

Test	Code	Geometry		Tensiometer			Ini. Cond.	Bound. Cond.
		r_R	z_D	Position	r_T	z_T	h_0	z_H
L1	L1.1	7.75	20.00	r	13.75	–2.50	–590	3.50
	L1.2	6.75	20.00	r	13.75	–0.80	–510	10.00
L2	L2.1	8.00	20.00	v	0.00	–12.00	–780	9.50
	L2.2	7.50	20.00	h	0.00	–11.00	–700	5.00
	L2.3	8.65	20.00	h	0.00	–11.00	–770	6.50
L3	L3.1	12.50	20.00	h	0.00	–12.00	–620	6.00
	L3.2	10.25	20.00	h	0.00	–10.00	–530	5.00
L4	L4.1	11.50	20.00	h	0.00	–9.50	–350	5.00
	L4.2	7.75	20.00	r	12.50	1.50	–250	10.00
L5	L5.1	9.00	20.00	r	15.00	–2.50	–610	6.00
	L5.2	8.00	20.00	r	14.00	–3.50	–680	6.00
	L5.3	7.50	20.00	r	–1.00	13.00	–380	7.00
	L5.4	7.25	20.00	r	16.00	–3.00	–710	6.00
	L5.5	6.75	20.00	v	0.00	–9.50	–530	10.00
	L5.6	3.00	20.00	r	10.00	2.00	–390	5.00
	L5.7	3.00	20.00	r	15.00	0.50	–490	20.00

RESULTS

Physical characterizations

Table 2 presents physical properties of samples collected at each location (sites L1 to L5). The classification in the third column reflects the weathering profile of the residual soils in Rio de Janeiro in terms of M (mature), Y (young) and S (saprolitic), according to Fig. 1. Multiple samples were collected at several locations for soil physical measurements. The dry bulk density ρ_d (g/cm^3), and porosity, φ, are listed in the last two columns of Table 2. Particle size distributions of the samples indicated a relative high percentage of gravel for the saprolitic soils. As expected, and visually illustrated in Fig. 1, such soils contain much material that preserves the microfabric and volume of the parent rock (Lacerda, 2010). The younger (lateritic) and mature residual soils showed a much more porous structure and higher clay and silt contents. These textural differences between the layered residual soils are noticeable when comparing samples from the same location, for instance from sites L1 and L4. The data in Table 2 for samples at locations L2, L3 and L4 closely agree with previous studies at the same sites by Maciel (1991), Carvalho (2012) and Buback (2008), respectively.

Monitored infiltration test

We now detail results of the infiltration tests at the five locations (L1 through L5). Fig. 7 compares observed (points) and simulated (lines) pressure head data, with results shown in color that match those in Fig. 3 for the mature (green), young (red), and saprolitic (blue) soils. Regardless of the location and residual soil type, the plots show excellent agreement between the simulated and observed pressure heads. The $h(t)$ curves show constant values until arrival of the moisture front at the tensiometer cup, at which time the pressure heads increase and eventually plateau at saturation. The saprolitic soils show much sharper wetting fronts, a characteristic of their coarser texture. One exception is test L2.3, which showed a more gradual increase in the pressure head with time. The moisture fronts of the young and mature residual soils were fairly similar and much more gradual than those of the saprolitic soils. This is an important finding in that it reflects the hydraulic heterogeneity of residual soils in Rio de Janeiro, to be supported here later also by the estimated $\theta(h)$ and $K(h)$ functions. The total time to execute the field experiments varied from about 2.2 h at location L1, to 1.6 h at locations L2 and L3, to less than an hour at the other sites. These times obtained are less than those found by Šimůnek et al. (1999) for hypothetical but very representative tension disc infiltration tests, which lasted between 4.5 and 5.5 hours.

Fig. 7a shows results of the infiltration process for the saprolitic (L1.1) and mature (L1.2) residual soils in the Campo Grande district (Fig. 3). The relatively large differences between the shapes of the wetting fronts of tests L1.1 and L1.2 reflect the nature of these two soils. The two tests, executed on the same soil profile, differ substantially in their infiltration characteristics. Although Table 1 highlights important differences in terms of depth of the tensiometers (L1.1 is positioned below L1.2), and the initial pressure head in the soil profile (L1.1 is higher with respect to site L1.2, leading to a higher initial hydraulic gradient), Fig. 7a shows earlier arrival of the wetting front for test L1.1. This result agrees well with the textural characteristics of each residual soil. In fact, the coarse nature of the saprolitic soil (L1.1) enables a significant fraction of the infiltrated water to move rapidly.

Fig. 7b compares the S-shaped infiltration curves of the saprolitic soils at the Joá site. The well-graded soil of sample L2.1 (Table 2) showed a much more gradual moisture front as indicated by the solid line in Fig. 7b, as compared with the more coarse-grained samples of L2.2 and L2.3. This finding can be explained in part by the considerable variability in the particle size distribution and mineralogy of saprolitic soils in Rio de Janeiro (Lacerda, 2010), in that some of the soils undergo more weathering to lead to higher clay contents (but usually still below 10%), thereby affecting the infiltration rate.

Table 2. Classification and physical properties of the residual soils sampled at different locations in Rio de Janeiro. Gr = Gravel, Sa = Sand, Si = Silt, Cl = Clay, ρ_d = Dry density, φ = Porosity, Y = Young residual soil, M = Mature residual soil, S = Saprolitic residual soil.

Test	Code	Soil class	Physical properties					
			Gr (%)	Sa (%)	Si (%)	Cl (%)	ρ_d (g/cm^3)	φ
L1	L1.1	S	4.1	85.6	7.6	2.7	1.33	0.51
	L1.2	M	0.4	72.9	18.9	7.8	1.35	0.50
L2	L2.1	S	25.1	47.4	12.8	14.7	1.39	0.48
	L2.2	S	12.0	77.0	6.1	4.9	1.39	0.51
	L2.3	S	12.0	77.0	6.1	4.9	1.39	0.51
L3	L3.1	Y	0.4	61.6	36.6	1.3	1.27	0.55
	L3.2	Y	0.4	61.6	36.6	1.3	1.27	0.55
L4	L4.1	Y	14.9	64.6	16.9	3.5	1.60	0.41
	L4.2	M	0.9	41.3	34.0	23.8	1.26	0.54
L5	L5.1	S	9.7	75.2	13.0	2.1	1.26	0.49
	L5.2	S	9.7	75.2	13.0	2.1	1.26	0.53
	L5.3	Y	0.9	57.6	28.5	13.0	1.58	0.41
	L5.4	S	5.0	61.4	26.1	7.5	1.21	0.54
	L5.5	M	1.9	49.7	39.5	8.9	1.51	0.43
	L5.6	M	1.9	49.7	39.5	8.9	1.51	0.44
	L5.7	Y	8.6	49.5	11.9	30.3	1.60	0.40

Since our measurements of the hydraulic properties did not reveal a single best and fastest setup for the experiments, arguably due to the distinct geometries and boundary conditions we adopted, further studies are needed to establish a good balance between the test setup, the accuracy of the measurements, and the required time to get reliable data for the inverse analysis. But the times required for our experiments (shown in the plots of Fig. 7) are far less than those required for most field experiments focusing on in-situ measurements of the unsaturated soil hydraulic properties.

Water retention and unsaturated hydraulic conductivity curves

Table 3 summarizes the soil hydraulic parameters optimized with the HYDRUS software for each test. The optimized VGM parameters were used to construct the water retention curve for all experiments (Fig. 8). Fig. 8a shows $\theta(h)$ functions derived for the experiments at site L1. The resulting retention curves for each experiment are consistent with the infiltration curves; they define different saturation trajectories but converge to approximately the same saturated water content.

Notice that we plotted only the wetting curves and did not consider hysteresis. The $\theta(h)$ function estimated from test L1.2 gave higher water contents over almost the entire pressure head range than those from test L1.1. The largest difference between the two tests is about 0.2 cm^3/cm^3 and occurs at the residual pressure head. The saprolitic residual soil (L1.1) showed a lower air entry value ($\alpha = 0.00841$ cm^{-1}) and a steeper slope of the $\theta(h)$ function at intermediate (negative) pressure heads (n = 1.81), in accordance with the higher amount of gravel and sand contents of such soils (van Genuchten, 1980).

Fig. 8b presents the $\theta(h)$ functions we obtained for the saprolitic soils at site L2. Experiments L2.2 and L2.3 exhibited very similar shapes of the retention function, similar as those of the saprolitic soil shown in Fig. 8a. The higher amount of fine material (12.8% of silt and 14.7% of clay contents) for the soil at location L2.1 compared to the other tests (6.1% of silt and 4.9% of clay contents) affected considerably the shape of the $\theta(h)$ function. This is reflected by the relatively low values of α (0.00318 cm^{-1}, indicative of a higher air entry values) and n (1.72, indicative of a broader pore-size distribution). The soil water retention function of experiment L2.1 very closely matched independent laboratory data from Maciel (1991) using the filter paper test. Results of the relatively similar retention functions derived for the mature residual soils at L3 site also indicated close agreement between our filter paper measurements and the estimated $\theta(h)$ function (Fig. 8c).

Fig. 8e displays the soil water retention functions obtained for the three typical residual soil classes of Rio de Janeiro.

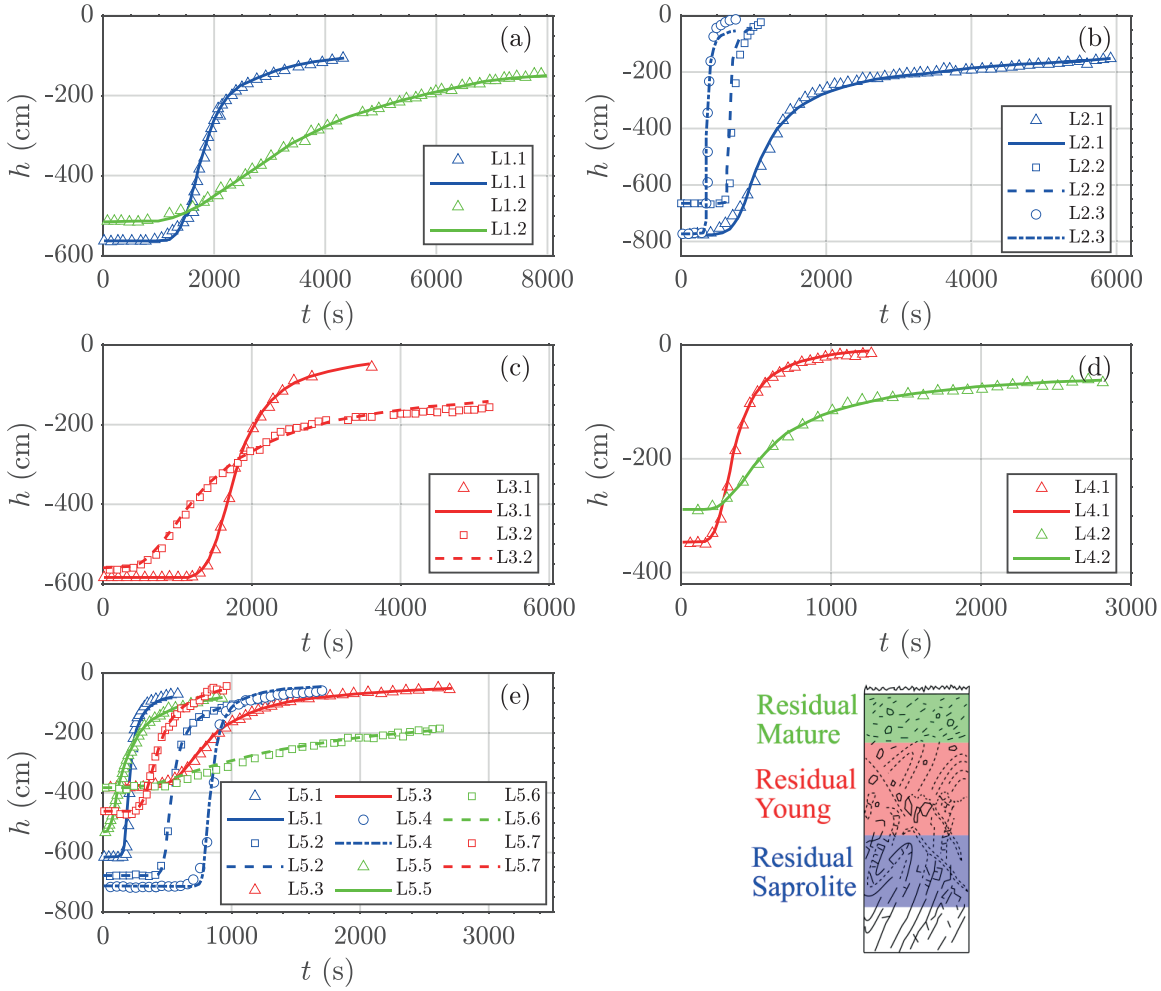

Fig. 7. Transient evolution of observed pressure heads (data points) using the monitored infiltration test at locations L1 (a), L2 (b), L3 (c), L4 (d), and L5 (e) for the mature (red), young (green), and saprolitic (blue) residual soils. Lines represent the optimized solutions obtained with the HYDRUS software.

Table 3. Summary of the estimated VGM parameters obtained using inverse modeling of the monitored infiltration test data.

Test	Code	Soil class	θ_r ($cm^3\ cm^{-3}$)	θ_s ($cm^3\ cm^{-3}$)	α (cm^{-1})	n (–)	K_s ($cm\ s^{-1}$)
L1	L1.1	S	0.051	0.51	0.00841	1.81	0.0001190
	L1.2	M	0.051	0.50	0.00262	1.15	0.0000231
L2	L2.1	S	0.039	0.48	0.00318	1.72	0.0001290
	L2.2	S	0.065	0.51	0.02250	2.68	0.0009930
	L2.3	S	0.065	0.51	0.01810	2.76	0.0024500
L3	L3.1	Y	0.007	0.55	0.00899	1.28	0.0003090
	L3.2	Y	0.007	0.55	0.00266	1.23	0.0000337
L4	L4.1	Y	0.078	0.41	0.00534	1.16	0.0003520
	L4.2	M	0.030	0.54	0.00468	1.45	0.0000592
L5	L5.1	S	0.045	0.49	0.01000	1.54	0.0013200
	L5.2	S	0.045	0.53	0.01010	2.02	0.0007140
	L5.3	Y	0.051	0.41	0.00990	1.30	0.0001690
	L5.4	S	0.051	0.54	0.01850	1.90	0.0018000
	L5.5	M	0.078	0.43	0.00120	1.18	0.0005050
	L5.6	M	0.078	0.44	0.00105	1.20	0.0000073
	L5.7	Y	0.038	0.40	0.00635	1.31	0.0005780

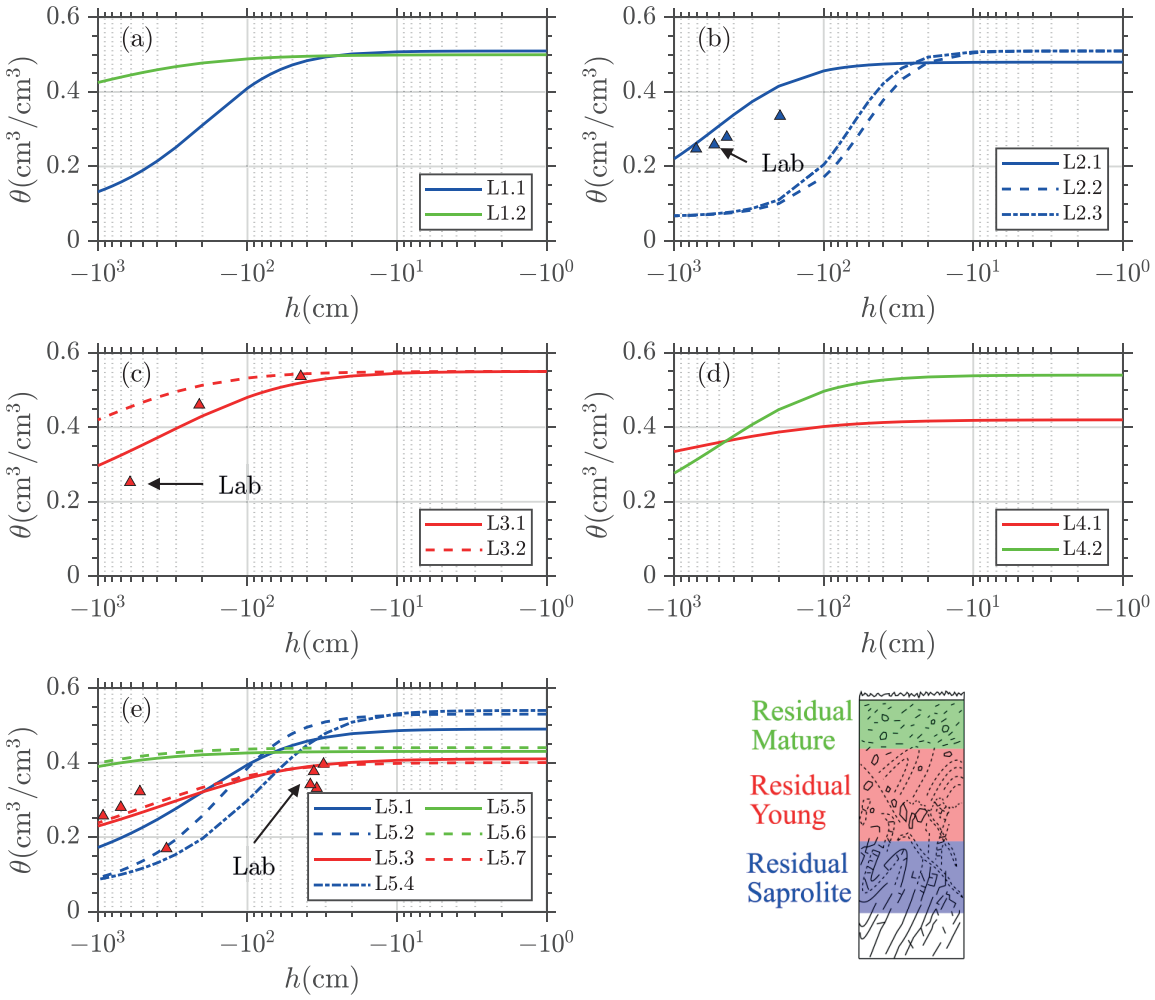

Fig. 8. Water retention functions of mature (green), young (red), and saprolitic (blue) residual soils derived with the HYDRUS software for five different measurement locations on hillslopes of Rio de Janeiro, Brazil: L1 (a), L2 (b), L3 (c), L4 (d), and L5 (e). Results obtained with independent filter paper tests are indicated with filled symbols.

Experiments L5.1 and L5.2 were found to have the same grain-size distribution (Table 2), but different porosity values (φ = 0.49 and 0.53, respectively). The L5.1 and L5.2 tests produced almost identical α values (0.0100 and 0.0101 cm^{-1}, respectively), but different n values (1.54 and 2.02), thereby revealing that the higher porosity caused more rapid changes in the moisture content of the saprolitic soils. Experiments L5.3 and L5.4 were executed at the same site, but approximately 200 meters from each other. The soil water characteristic curves of these two tests provide some useful insights about the moisture-pressure head relationships of the young (L5.3) and saprolitic (L5.4) residual soils in the area. In fact, the lower α value (0.0099 cm^{-1}) and the smoother slope (n = 1.3) of the $\theta(h)$ function of L5.3, and the fact that most of the infiltration at L5.4 occurred over a narrow suction range, appears to define effective ranges of the soil hydraulic parameters for such soils. Additionally, the filter paper results from Oliveira (2013) for similar soils at location L5.3 indicated good agreement with our estimated retention curve. Finally, Fig. 8e also highlights that the retention functions of tests L5.5, L5.6 and L5.7 closely matched the $\theta(h)$ functions of each corresponding soil class.

Fig. 9 illustrates the unsaturated hydraulic conductivity functions obtained with the inverse modeling approach. As expected, Fig. 9a shows that the saprolitic soil at the L1.1 site exhibited a higher saturated hydraulic conductivity (K_s = 1.19·10^{-4} cm s^{-1}) and a lower permeability as the soil dried out.

The mature residual soil of experiment L1.2 clearly showed lower K_s-values, but at lower pressure heads (–400 cm) the fine-grained soil exceeded the conductive of the saprolitic soil. The saprolitic residual soils demonstrated similar $K(h)$ functions in Fig. 9b, except for the L2.1 test at a very low suction range. This plot also illustrates that the K_s values of these saprolitic soils (1.29·10^{-4} < K_s < 2.45·10^{-3} cm s^{-1}) had very similar mean values (K_s = 2.47·10^{-4} cm s^{-1}) as obtained by Maciel (1991) for 12 laboratory permeability tests (solid blue point).

The $K(h)$ functions shown in Fig. 9c display results of the young residual soils of Duque de Caxias, Rio de Janeiro. As can be noticed, the unsaturated hydraulic conductivity functions are fairly similar in the low pressure head range, but become progressively different towards saturation. Indeed, the saturated hydraulic conductivity of these two soils differed by one order of magnitude between K_s = 3.09·10^{-4} cm s^{-1} (L3.1) and K_s = 3.37·10^{-4} cm s^{-1} (L3.2), probably caused by spatial variability. Fig. 9c also includes field K_s tests with the help of a Guelph permeameter (K_s = 2.02·10^{-4} cm s^{-1}), a flexible wall permeameter (K_s = 8.00·10^{-7} cm s^{-1}) and laboratory procedures by Carvalho (2012) (K_s = 2.00·10^{-6} cm s^{-1}) further highlighting the variability in K_s. This finding agrees with previous K_s measurements by Vieira and Fernandes (2004), who observed abrupt changes in K_s in some of the same soil profiles as studied here.

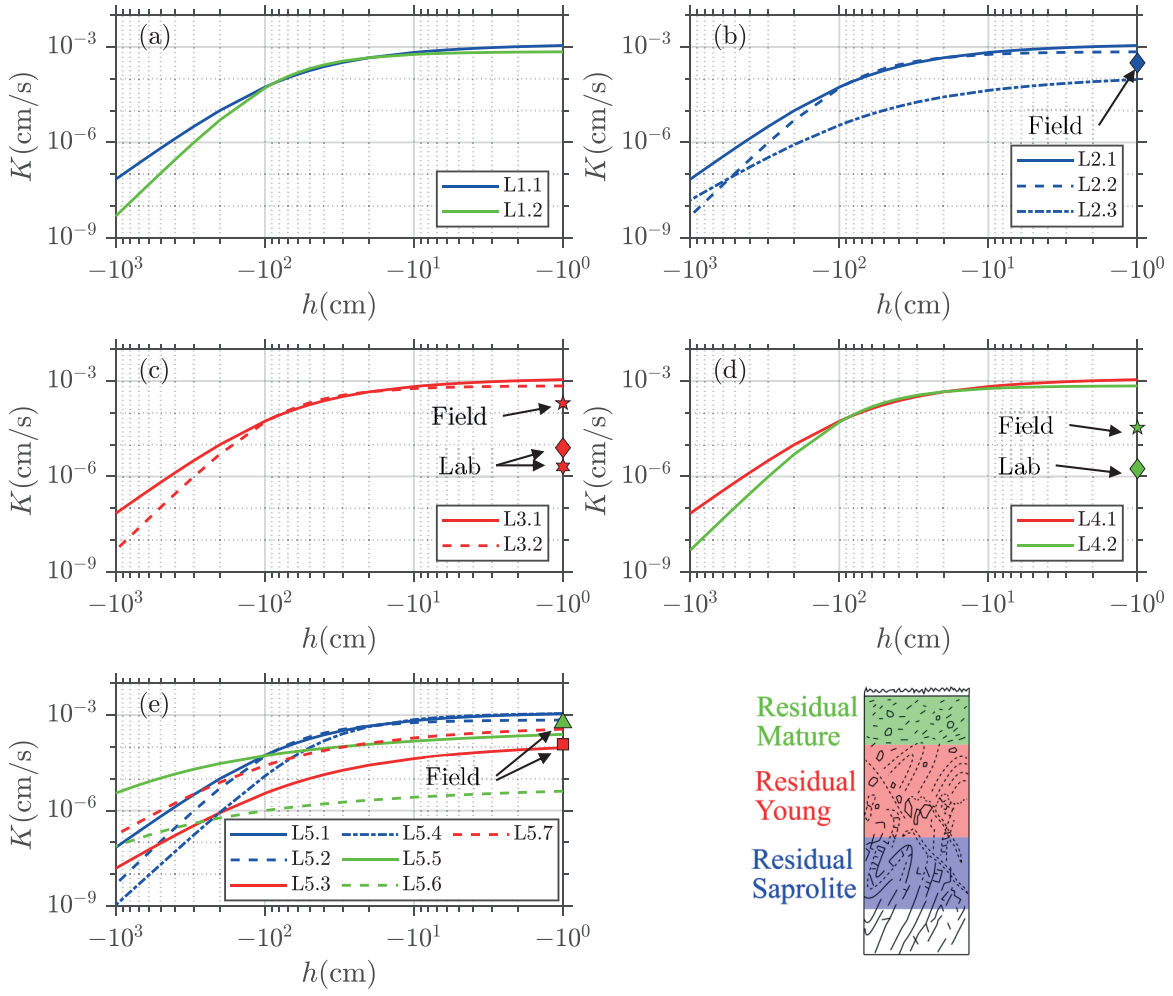

Fig. 9. Unsaturated hydraulic conductivity functions of mature (green), young (red), and saprolitic (blue) residual soils derived with the HYDRUS software for five different locations on hillslopes of Rio de Janeiro, Brazil: L1 (a), L2 (b), L3 (c), L4 (d), and L5 (e). Results obtained with independent field and laboratory tests are separately indicated by arrows and filled symbols.

For instance, they reported an increase in K_s values of two orders of magnitude over short distances (0.30 m). As depicted in Fig. 9d, the coarse-grained soil of experiment L4.1 presented a higher K_s value ($3.52 \cdot 10^{-4}$ cm s^{-1}) compared to the fine-grained soil ($5.92 \cdot 10^{-5}$ cm s^{-1}). Guelph permeameter field experiments on the fine-grained soil (L4.2) revealed close agreement ($K_s = 3.42 \cdot 10^{-5}$ cm s^{-1}) with the monitored infiltration test. Yet, as pointed out in Fig. 9d, laboratory test provided by Carvalho (2012) indicated a K_s value that was one order of magnitude lower ($1.80 \cdot 10^{-6}$ cm s^{-1}), again demonstrating the spatial variability in K_s of gneissic soils in Rio de Janeiro.

The $K(h)$ functions shown in Fig. 9e nicely reflect the transition between the unsaturated hydraulic conductivity functions of the three different soil types obtained in the present study. Again, spatial variability in K_s is evident from a visual inspection of the plots for experiments L5.5 and L5.6, both executed on mature residual soils. The estimated saturated hydraulic using inverse modeling for L5.5 ($K_s = 5.05 \cdot 10^{-4}$ cm s^{-1}) was higher than for L5.6 ($K_s = 7.30 \cdot 10^{-6}$ cm s^{-1}). One possible reason for the discrepancy in the $K(h)$ functions of tests L5.5 and L5.6 is the distinct geometric configuration used in the two experiments (Table 1). Since the infiltration tests were executed using different radial and vertical settings, differences may have been caused by anisotropy in the soil hydraulic properties. Still, our Guelph tests performed at the same locations L5.5 and L5.3 indicated quite similar result for the mature ($K_s = 5.76 \cdot 10^{-4}$ cm s^{-1}) and young residual ($K_s = 1.21 \cdot 10^{-4}$ cm s^{-1}) soils, respectively.

Overall, the filter paper tests indicated adequate agreement with the estimated parameters using the monitored infiltration test. Estimates of the saturated hydraulic conductivity indicated consistent results for the field measurements (i.e., the monitored infiltration test and Guelph permeameter tests). Laboratory tests, however, revealed large discrepancies (up to two orders of magnitude) compared with the field results. It is known that under field conditions, macropores and cracks increase the saturated hydraulic conductivity. These conditions may be particularly difficult to reproduce in the laboratory on small soil samples (Scharnagl et al., 2011).

Effective soil hydraulic properties

We conclude this paper with Fig. 10, which displays effective soil hydraulic properties for the residual soils of Rio de Janeiro, Brazil. The various HYDRUS-2D analyses of the VGM parameters were used to characterize the mean (effective) properties of the $\theta(h)$ and $K(h)$ functions. Results are presented in Fig. 10, which shows the mean (solid lines) and 95% bounds (shaded regions) of the water retention (a) and hydraulic conductivity (b) functions. The $\theta(h)$ functions of the mature (green) and young (red) residual soils suggest excellent water holding capacities of these soils, with pressure heads that must be below –80 cm for air to enter the pores. This finding is consistent with our soil textural data, which demonstrate relatively high percentages of silt and clay, while also being supported by previous results by Gomes et al. (2017) in the same region. Similar results were obtained by Xia et al. (2019), who found that the upper two soil layers of a granitic residual soil in China also had a stronger water-holding capacity. The saprolitic residual soils in our study demonstrated a comparatively narrow

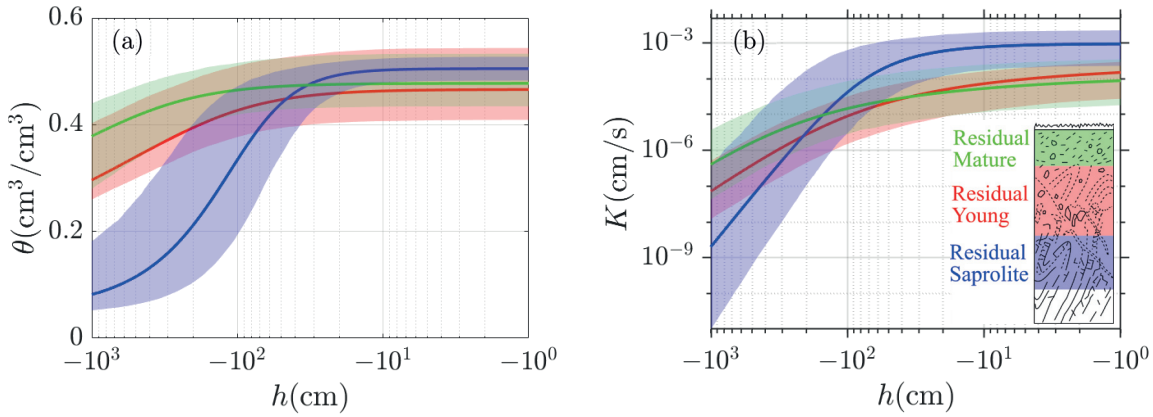

Fig. 10. Estimated effective soil water retention (a) and hydraulic conductivity (b) functions of the residual soils of Rio de Janeiro, including mean values (solid lines) and the 95% confidence intervals as derived with the HYDRUS software using a series of monitored infiltration test for mature (green), young (red), and saprolitic (blue) soils.

Table 4. Estimated effective VGM soil hydraulic parameters of mature (M), young (Y), and saprolitic (S) residual soils of Rio de Janeiro, Brazil.

Class	Summary θ-statistics	θ_r (cm^3 cm^{-3})	θ_s (cm^3 cm^{-3})	α (cm^{-1})	n (–)	K_s (cm s^{-1})
M	Min.	0.030	0.43	0.0011	1.15	0.00000733
	Max.	0.078	0.54	0.0047	1.45	0.00050500
	Mean	0.059	0.48	0.0024	1.24	0.00014900
Y	Min	0.007	0.40	0.0027	1.16	0.00003370
	Max	0.078	0.55	0.0099	1.31	0.00057800
	Mean	0.036	0.47	0.0066	1.26	0.00028800
S	Min.	0.039	0.48	0.0032	1.54	0.00011900
	Max.	0.065	0.53	0.0225	2.76	0.00250000
	Mean	0.052	0.51	0.0120	2.09	0.00095400

pore-size distribution, with most drainage occurring in a relatively narrow suction range. These soils are characterized by relatively large values of α (low air entry values) and n, the latter reflected by higher $K(h)$ values and more rapidly decreasing $K(h)$ functions as the soil dries out. Table 4 lists summary statistics of the estimated effective VGM soil hydraulic parameters of the studied residual soils.

The relatively large confidence intervals of the $\theta(h)$ and $K(h)$ functions are related to the hydraulic heterogeneity of residual soils in Rio de Janeiro. The wide intervals suggest that one should not rely on single unique estimates of the VGM parameters in the presence of heterogeneities and natural variability of the soil hydraulic properties, also in view of measurement errors of the experimental data. Indeed, practical experience suggests that it is typically difficult to find effective soil water retention and hydraulic conductivity functions for residual soils (Kassim et al., 2012; Peranić et al., 2018; Rahardjo and Satyanaga, 2019; Xia et al., 2019). Still, the derived effective VGM soil hydraulic parameters for residual soils of Rio de Janeiro may be useful for regional slope stability studies, which frequently depend on such data to model subsurface water flow processes (Camargo et al., 2016; Gerscovich et al., 2006; Gomes et al., 2017). Moreover, our results demonstrate that young and mature residual soils have similar hydraulic properties, indicating that further numerical simulations could assume uniform hydraulic properties for these soil layers.

CONCLUSIONS

The saprolitic soils in this study exhibited high saturated hydraulic conductivities and large air-entry pressures (low α values), with imbibition occurring over a relatively narrow pressure head range. The young and mature residual soils showed good water holding capacities, with pressure heads that must be low for air to enter the pores, and relatively high percentages of silt and clay. Differences in the effective soil properties obtained for the distinct residual soil classes can be quite large, reiterating the need for a careful treatment of hydraulic heterogeneity, especially in regional slope stability studies. Results derived from this study should help to better inform engineers and others about the hydraulic parameters of soils in the landslide-prone areas of Rio de Janeiro, and possibly in other regions with similar geologic settings and climate conditions.

The monitored infiltration test offers a rapid, accurate, and simple way to derive the hydraulic properties of unsaturated soils. The field approach only demands a tensiometer to measure pressure heads below the infiltration front triggered by a Mariotte bottle, supplying constant water at the top edge of the soil profile. The test is fast since it does not need steady-state flow to allow inverse modeling, uses a simple geometry for the field experiments, and is versatile in that it can be quickly conducted on steep slopes. Our results demonstrate that the monitored infiltration test provides a viable approach to measure the hydraulic functions for a variety of young, mature, and saprolitic residual soils. Comparisons with different laboratory (such as filter paper) and field (including Guelph permeameter) tests sustained this conclusion. More substantial investigations may be needed to improve parameter identifiability, such as increasing the number and locations of observations, and possible extensions to anisotropic and more structured soil systems.

*Acknowledgements.*The project presented in this article is supported by the Brazilian National Council for Scientific and Technological Development, CNPq (Conselho Nacional de Desenvolvimento Científico e Tecnológico). We are also very grateful to Raquel Q. Velloso for her help with the conceptualization and implementation of the Monitored Infiltration Test.

REFERENCES

ABNT, 2016a. Soil - granulometric analysis: procedure. NBR 7181. Brazilian Association of Technical Standards.

ABNT, 2016b. Soil - preparation for compaction and characterization tests. NBR 6457. Brazilian Association of Technical Standards.

ASTM, 2013. Standard Test Method for Measurement of Soil Potential (Suction) Using Filter Paper. ASTM D5298-10. Am. Soc. Testing and Materials. DOI: 10.1520/D5298-10

ASTM, 2016. Standard Test Methods for Measurement of Hydraulic Conductivity of Saturated Porous Materials Using a Flexible Wall Permeameter. ASTM D5084-16a. Am. Soc. for Testing and Materials. DOI: 10.1520/D5084-16A

Aydin, A., 2006. Stability of saprolitic slopes: nature and role of field scale heterogeneities. Natural Hazards and Earth System Sci., 6, 89–96. DOI: 10.5194/nhess-6-89-2006

Bells, F. (Ed.), 2005. Engineering Geology, Problematic Soils. Elsevier. DOI: 10.1016/B0-12-369396-9/00221-5

Buback, J., 2008. Caracterização físico-química-minerológica e micromorfolóogica de um perfil de alteraçao de rocha alcalina do Rio de Janeiro [Residual soil alkaline origin characterization at the Tangá city, Rio de Janeiro]. MS Thesis. Pontifical Catholic University of Rio de Janeiro, Brazil.

Camargo, J., Velloso, R., Vargas, E., 2016. Numerical limit analysis of three- dimensional slope stability problems at catchment scale. Acta Geotechnica, 11, 1369–1383. DOI: 10.1007/s11440-016-0459-3

Carvalho, T., 2012. Desenvolvimento de um sistema de medição de variação de volume total de amostras triaxiais não-saturadas e avaliação do efeito de processos de saturação no comportamento de solos saprolíticos [Development of a total volume change measuring system for unsaturated triaxial samples and evaluation of the effect of saturation procedures on the be- haviour of saprolitic soils]. PhD Thesis. Pontifical Catholic University of Rio de Janeiro, Brazil.

Chen, P., Wei, C., Yi, P., Ma, T., 2017. Determination of hydraulic properties of unsaturated soils based on nonequilibrium multistep outflow experiments. J. Geotechn. Geoenviron. Eng., 143, 1, Article Number: 04016087. DOI: 10.1061/(ASCE)GT.1943-5606.0001598

Fernandes, N.F., Guimarães, R.F., Gomes, R.A.T., Vieira, B.C., Montgomery, D.R., Greenberg, H., 2004. Topographic controls of landslides in Rio de Janeiro: field evidence and modeling. Catena, 55, 163–181. DOI: 10.1016/ S0341-8162(03)00115-2

Gerscovich, D.M.S., Vargas Jr., E.A, de Campos, T.M.P., 2006. On the evaluation of unsaturated flow in a natural slope in Rio de Janeiro, Brazil. Eng. Geol., 88, 23–40. DOI: 10.1016/j.enggeo.2006.07.008

Gomes, G.J.C., Vrugt, J.A., Vargas Jr., E.A., 2016. Toward improved prediction of the bedrock depth underneath hillslopes: Bayesian inference of the bottom- up control hypothesis using high-resolution topographic data. Water Resour. Res., 52, 3085–3112. DOI: 10.1002/2015WR018147

Gomes, G.J.C., Vrugt, J.A, Vargas Jr., E.A., Camargo, J.T., Velloso, R.Q., van Genuchten, M.T., 2017. The role of uncertainty in bedrock depth and hydraulic properties on the stability of a variably-saturated slope. Computers & Geotechnics,

88, 222–241. DOI: 10.1016/j.compgeo.2017.03.016

Gomes, R.A.T, Guimarães, R.F., Carvalho, O.A., Fernandes, N.F., Vargas Jr., E.A., Martins, E.S., 2008. Identification of the affected areas by mass movement through a physically based model of landslide hazard combined with an empirical model of debris flow. Natural Hazards, 45, 197–209. DOI: 10.1007/ s11069-007-9160-z

Gonçalves, R.D., Teramoto, E.H, Engelbrencht, B.Z., Soto, M.A.A., Chang, H.K., van Genuchten, M.T., 2019. Quasi-saturated layer: Implications for estimating recharge and groundwater modeling. Groundwater, 58, 432–440. DOI: 10. 1111/gwat.12916

Inoue, M., Šimůnek, J., Hopmans, J.W., Clausnitzer, V., 1998. In situ estimation of soil hydraulic functions using a multi-step soil-water extraction technique. Water Resour. Res., 34, 1035–1050. DOI: 10.1029/98WR00295

Kassim, A., Gofar, N., Lee, L.M., Rahardjo, H., 2012. Modeling of suction distribution in an unsaturated heterogeneous residual slope. Eng. Geol., 131–132, 70–82. DOI: 10.1016/j.enggeo.2012.02.005

Lacerda, W., 2010. Shear strength of soils derived from the weathering of granite and gneiss in Brazil. Geological Society, London, Eng. Geol. Special Publications 3, 167–182. DOI: 10.1144/EGSP23.10

Li, W.C., Dai, F.C., Wei, Y.Q., Wang, M.L., Min, H., Lee, L.M., 2016. Implication of subsurface flow on rainfall-induced landslide: a case study. Landslides, 13, 1109–1123. DOI: 10.1007/s10346-015-0619-9

Liang, W.L., Uchida, T., 2014. Effects of topography and soil depth on saturated-zone dynamics in steep hillslopes explored using the three-dimensional Richards' equation. J. Hydrol., 510, 124–136. DOI: 10.1016/j.jhydrol.2013.12.029

Maciel, I., 1991. Aspectos Microestruturais e Propriedades Geomecánicas de um Perfil de Solo Residual de Gnaisse Facoidal [Micro-structural aspects and geomechanical properties of a residual soil profile]. Master's thesis. Pontifical Catholic University of Rio de Janeiro, Brazil.

Oliveira, C., 2013. Avaliação de mecanismos de ruptura associados aos escorregamentos da Prainha e Condomínio em Nova Friburgo, Rio de Janeiro [Assessment of failure mechanisms of the Prainha and Condomínio landslides, in Nova Friburgo, Rio de Janeiro]. Master's Thesis. Pontifical Catholic University of Rio de Janeiro, Brazil.

Peranić, J., Arbanas, Z., Cuomo, S., Maček, M., 2018. Soil-water characteristic curve of residual soil from a flysch rock mass. Geofluids. DOI: 10.1155/2018/6297819

Peranić, J., Moscariello, M., Cuomo, S., Arbanas, Z., 2020. Hydro-mechanical properties of unsaturated residual soil from a flysch rock mass. Eng. Geol., 269, Article Number: 105546. DOI: 10.1016/j.enggeo.2020.105546

Peters, A., Iden, S.C., Durner, W., 2015. Revisiting the simplified evaporation method: Identification of hydraulic functions considering vapor, film and corner flow. J. Hydrol., 527, 531–542. DOI: 10.1016/j.jhydrol. 2015.05.020

Rahardjo, H., Satyanaga, A., 2019. Sensing and monitoring for assess- ment of rainfall-induced slope failures in residual soil. Proc. Inst. Civil Eng., Geotechnical Engineering 176, 496–506. DOI: 10.1680/jgeen.18.00208

Reynolds, W.D., Elrick, D.E., 1986. A method for simultaneous in situ measurement in the vadose zone of field-saturated hydraulic conductivity, sorptivity and the conductivity-pressure head relationship. Ground Water Monitoring & Remediation, 6, 84–95. DOI: 10.1111/j.1745-6592.1986.tb01229.x

Rosi, A., Canavesi, V., Segoni, S., Nery, T.D., Catani, F., Casagli., N., 2019. Landslides in the mountain region of Rio de Janeiro: A proposal for the semi-automated definition of multiple rainfall thresholds. Geosci., 9, 5, Article Number: 203. DOI: 10.3390/geosciences9050203

Schaap, M.G., Leij, F.J., van Genuchten, M.T., 2001. Rosetta: a computer program for estimating soil hydraulic parameters with hierarchical pedotransfer functions. J. Hydrol., 251, 163–176. DOI: 10.1016/ S0022-1694(01)00466-8

Scharnagl, B., Vrugt, J.A., Vereecken, H., Herbst, M., 2011. Inverse modelling of in situ soil water dynamics: investigating the effect of different prior distributions of the soil hydraulic parameters. Hydrol. Earth Syst. Sci., 15, 3043–3059. DOI: 10.5194/hess-15-3043-2011

Šimůnek, J.J., van Genuchten, M.T., 1996. Estimating unsaturated soil hydraulic properties from tension disc infiltrometer data by numerical inversion. Water Resour. Res., 32, 2683–2696. DOI: 10.1029/96WR01525

Šimůnek, J.J., van Genuchten, M.T., Gribbs, M.M., Hopmans., J.W., 1998. Parameter estimation of unsaturated soil hydraulic properties from transient flow processes. Soil Tillage Res., 47, 27–37. DOI: 10.1016/S0167-1987(98) 00069-5

Šimůnek, J., Kodešová, R., Gribb, M.M., van Genuchten., M.T., 1999. Estimating hysteresis in the soil water retention function from cone permeameter experiments. Water Resour. Res., 35, 1329–1345. DOI:10.1029/ 1998WR900110

Šimůnek, J., van Genuchten, M.T., Šejna, M., 2012. Hydrus: Model use, calibration and validation. Trans. ASABE, 55, 1261–1274. DOI: 10.13031/2013.42239

Šimůnek, J.J., van Genuchten, M.T., Šejna, M., 2016. Recent developments and applications of the Hydrus computer software packages. Vadose Zone J., 15, 1–25. DOI: 10.2136/vzj2016.04.0033

van Genuchten, M.T., 1980. A closed-form equation for predicting the hydraulic conductivity of unsaturated soils. Soil Sci. Soc. Am. J., 44, 892–898. DOI: 10.2136/sssaj1980.03615995004400050002x.

Velloso, R.Q., 2000. Estudo Numérico da Estimativa de Parâmetros Hidráulicos em Solos Não Saturados [Numerical Study of the Estimation of Hydraulic Parameters in Partially Saturated Soils]. Master's Thesis. Pontifical Catholic University of Rio de Janeiro, Brazil.

Vieira, B.C., Fernandes, N.F., 2004. Landslides in Rio de Janeiro: The role played by variations in soil hydraulic conductivity. Hydrol. Proc., 18, 791–805. DOI: 10.1002/hyp.1363

Vrugt, J.A., van Wijk, M.T., Hopmans, J.W., Šimůnek, J.J., 2001. One-, two-, and three-dimensional root water uptake functions for transient modeling. Water Resour. Res., 37, 2457–2470. DOI: 10.1029/2000WR000027

Vrugt, J.A., Schoups, G., Hopmans, J.W., C. Young, W.W., Harter, T., Bouten, W., 2004. Inverse modeling of large-scale spatially distributed vadose zone properties using global optimization. Water Resour. Res., 40, 6. DOI: 10.1029/ 2003WR002706

Vrugt, J.A, Stauffer, P.H., Wöhling, T., Robinson, B.A., Vesselinov, V.V., 2008. Inverse modeling of subsurface flow and transport properties: A review with new developments. Vadose Zone J., 7, 843–864. DOI: 10.2136/vzj2007. 0078

Xia, J., Cai, C., Wei, Y., Wu, X., 2019. Granite residual soil properties in collapsing gullies of south China: spatial variations and effects on collapsing gully erosion. Catena, 174, 469–477. DOI: 10.1016/j.catena.2018.11.015

Received 29 March 2022
Accepted 25 April 2022